Dissecting the Dynamic Conformations of the Metamorphic Protein Lymphotactin

ARTICLE *in* THE JOURNAL OF PHYSICAL CHEMISTRY B · SEPTEMBER 2014

Impact Factor: 3.3 · DOI: 10.1021/jp504997k · Source: PubMed

THE JOURNAL OF PHYSICAL CHEMISTRY B

Article

pubs.acs.org/JPCB

Dissecting the Dynamic Conformations of the Metamorphic Protein Lymphotactin

Sophie R. Harvey,[†] Massimiliano Porrini,[‡] Albert Konijnenberg,[†] David J. Clarke,[†] Robert C. Tyler,[§] Patrick R. R. Langridge-Smith,[†] Cait E. MacPhee,[∥] Brian F. Volkman,[§] and Perdita E. Barran*[,⊥]

[†]School of Chemistry and [∥]School of Physics and Astronomy, University of Edinburgh, West Mains Road, Edinburgh EH9 3JJ, United Kingdom

[‡]Institut Européen de Chimie et Biologie (IECB), CNRS UMR 5248 Chimie et Biologie des Membranes et des Nano-objets (CBMN), 33607 Pessac Cedex, France

[§]Department of Biochemistry, Medical College of Wisconsin, Milwaukee, Wisconsin 53226, United States

[⊥]School of Chemistry, Manchester Institute of Biotechnology, University of Manchester, Manchester M1 7DN, United Kingdom

Supporting Information

ABSTRACT: A mass spectrometer provides an ideal laboratory to probe the structure and stability of isolated protein ions. Interrogation of each discrete mass/charge-separated species enables the determination of the intrinsic stability of a protein fold, gaining snapshots of unfolding pathways. In solution, the metamorphic protein lymphotactin (Ltn) exists in equilibrium between two distinct conformations, a monomeric (Ltn10) and a dimeric (Ltn40) fold. Here, we use electron capture dissociation (ECD) and drift tube ion mobility-mass spectrometry (DT IM-MS) to analyze both forms and use molecular dynamics (MD) to consider how the solution fold alters in a solvent-free environment. DT IM-MS reveals significant conformational flexibility for the monomer, while the dimer appears more conformationally restricted. These findings are supported by MD calculations, which reveal how salt bridges stabilize the conformers in vacuo. Following ECD experiments, a distinctive fragmentation pattern is obtained for both the monomer and dimer. Monomer fragmentation becomes more pronounced with increasing charge state especially in the disordered regions and C-terminal α-helix in the solution fold. Lower levels of fragmentation are seen in the β-sheet regions and in regions that contain salt bridges, identified by MD simulations. The lowest charge state of the dimer for which we obtain ECD data ($[D+9H]^{9+}$) exhibits extensive fragmentation with no relationship to the solution fold and has a smaller collision cross section (CCS) than charge states 10−13+, suggesting a "collapsed" encounter complex. Other charge states of the dimer, as for the monomer, are resistant to fragmentation in regions of β-sheets in the solution fold. This study provides evidence for preservation and loss of global fold and secondary structural elements, providing a tantalizing glimpse into the power of the emerging field of native top-down mass spectrometry.

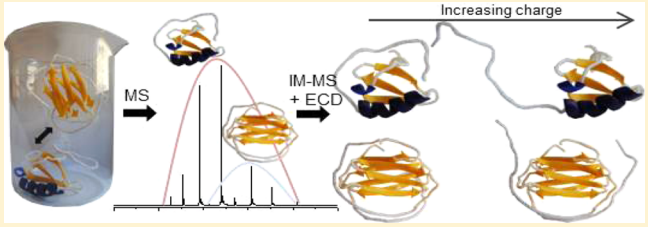

INTRODUCTION

Starting from Levinthal's paradox,[1] there have been many theoretical approaches to explain how a primary sequence encodes a protein fold, and while these differ, there is some consensus that both intrinsic and extrinsic factors come into play. The gas phase provides an excellent venue to distinguish these effects, and here, we use it to examine the metamorphic protein lymphotactin (Ltn). Ltn is a human chemokine, a small secreted signaling protein, which during immune response directs the migration of leukocytes toward areas of inflammation.[2,3] Ltn is a unique chemokine, the defining member of the XC subclass of this important family of proteins, which contain only one disulfide bond as opposed to the two normally found in other classes,[2] and comprises a unique extended C-terminal sequence that forms an intrinsically disordered tail. Ltn exists in equilibrium between two distinct conformations, a monomer that is preferred at 10 °C (Ltn10) and a dimer stabilized above 40 °C (Ltn40). Each form of this metamorphic protein is associated with a separate role in vivo.[4] Interconversion between these two folds involves a complete restructuring of the core residues.[5]

Since the development of soft ionization techniques such as electrospray ionization (ESI) and nano-ESI (n-ESI), mass spectrometry (MS) has become a valuable tool for structural analysis of proteins and protein complexes, and methods have been established that can preserve solution topologies.[6−9] Furthermore, theoretical studies have suggested that major secondary structural features of proteins can be preserved during transfer into the gas phase under ESI conditions.[10,11] Coupling of soft ionization techniques with gas-phase spectroscopic methods such as IR has begun to provide experimental evidence for

Received: May 21, 2014
Revised: September 26, 2014
Published: September 26, 2014

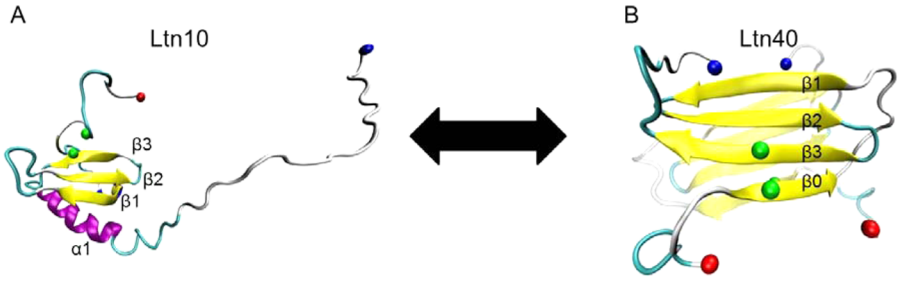

Figure 1. (A) Conserved chemokine fold of Ltn10: the equilibrium can be shifted toward this conformation at 10 °C with 200 mM NaCl, PDB 1J9O. Green spheres highlight the position of the disulfide bond. (B) Dimeric, GAG binding fold Ltn40: the equilibrium is shifted toward this conformation above 40 °C with 0 mM NaCl, PDB 2JP1. For clarity, the β-sheets of a single monomeric unit are labeled, with the monomer shown in solid coloring with the second monomer given a transparent color gradient. In both cases, the N-terminus is highlighted with a red sphere, and the C-terminus is highlighted with a blue sphere. Note that the PDB structure for Ltn40 does not contain the full disordered sequence; hence, this region is not shown in this figure.

preservation of structural motifs within proteins in the gas phase including α-helices.[12−15] There is, to date, less evidence for the retention of β-sheets in protein ions in the gas phase, although there are suggestive data from small-model peptides.[16,17] Successful transmission of proteins and their complexes into a mass spectrometer does not depend on the preservation of the secondary or tertiary fold, and indeed, there is much promise for the use of MS to study disordered proteins, with studies providing information on the coupled binding and folding of disordered regions in addition to different conformational distributions of disordered systems.[18−20] There is strong evidence for the retention of aspects of the tertiary fold and also for collapse and elongation of proteins. Because proteins are dynamic entities, all of these conformational states are potentially of interest.

Following gentle desolvation, a mass spectrometer is able to capture folded, unfolded, and partially unfolded states of proteins and protein complexes from solution and interrogate them using so-called "top-down" mass spectrometery.[21] Ltn possesses all classical elements of protein secondary structure (an α-helix in the Ltn10 form, β-sheets in both the monomer and the dimer, inter-β-sheet interactions in the dimer (Ltn40), as well as significant disordered regions) (Figure 1). Due to its metamorphic nature, all of these can be present under one set of solution conditions, existing as a mixture of monomer and dimer and the corresponding transitional intermediate states. The question we pose in this article is, can we capture and analyze all of these in the gas phase?

The combination of ion mobility spectrometry (IMS) and MS, known as ion mobility-mass spectrometry (IM-MS), has gained importance as a biophysical technique in recent years due to its ability to examine conformations adopted by proteins in the gas phase.[22−26] In IM-MS, ions are separated based on their mass-to-charge ratio in addition to their size and shape, the latter of which is defined by the experimentally derived collision cross section (CCS). The CCS provides coarse-grained information on conformations adopted by ions in the gas phase[27,28] that can be compared to solution coordinates obtained from protein databank (PDB) files or through molecular modeling.[29−31]

Recently, studies that combine IM-MS experiments with structural analysis by electron capture dissociation (ECD) have been presented, providing further insight into gas-phase protein and peptide conformations.[32,33] ECD is a fast, nonergodic fragmentation process with bond cleavage following electron capture occurring much faster than typical bond vibration.[34,35] Hence, ECD is thought not to perturb the higher-order structure of proteins. Further, there is compelling evidence for the absence of cleavage in regions containing α-helices (as shown by solution structures)[33,36] and also in those containing salt bridges. This suggests that noncovalent interactions that give rise to secondary structural elements prevent fragmentation in these regions and positions ECD as an attractive method by which to assess if secondary structures are retained in the gas phase for any given protein. Over the last couple of decades, ECD has been used in a number of elegant studies of protein folding, providing further proof for the presence of α-helices in the gas phase and information on their relative stability in a three-helix bundle.[36−40]

Here, we utilize drift tube (DT) IM-MS and ECD to probe the conformations adopted by the metamorphic protein Ltn (both as a monomer and as a dimer), in addition to a truncated form of Ltn (1−72) that contains the structural core of the protein but does not contain the intrinsically disordered C-terminus. We present ECD fragmentation maps that are distinctive fingerprints for each charge state of the monomer and dimer of this metamorphic, dynamic protein. Observations on the structure and stability of this chemokine in the absence of solvent are compared with findings from solution. This gas-phase approach provides a framework to examine order to disorder transitions that could be applied to study structures de novo.

EXPERIMENTAL SECTION

Protein Expression and Purification. All recombinant human wild type (WT) and 1−72 Ltn protein used in ECD and DT IM-MS investigations were expressed and purified as previously described.[41,42] The WT 72−93 construct, the disordered tail of the protein, was expressed using a his-tagged procedure, as previously described,[43] and after tag cleavage, it contained an additional two amino acids at its N terminus (GS). All expression vectors were verified by DNA sequencing. Purified proteins were frozen, lyophilized, and stored at −20 °C for subsequent study.

DT IM-MS. n-ESI was utilized for all IM-MS experiments. Sample solutions were ionized through a potential applied to a thin platinum wire inserted in a glass capillary. Nanoelectrospray tips were made in-house using thin-walled glass capillaries (i.d. 0.5 mm) using a Flaming/Brown micropipette puller (Sutter Instrument Company, Novato, CA, U.S.A.). All DT IM-MS measurements were performed on an in-house-modified Q-TOF (Micromass U.K. Ltd.), adapted in order to carry out separations based on an ion's mobility and to enable the temperature-dependent CCS to be determined from the measured m/z selected arrival time distributions (ATDs). This is possible via the inclusion of a 5.1 cm long copper drift cell and supplementary ion optics situated post source but before the quadrupole

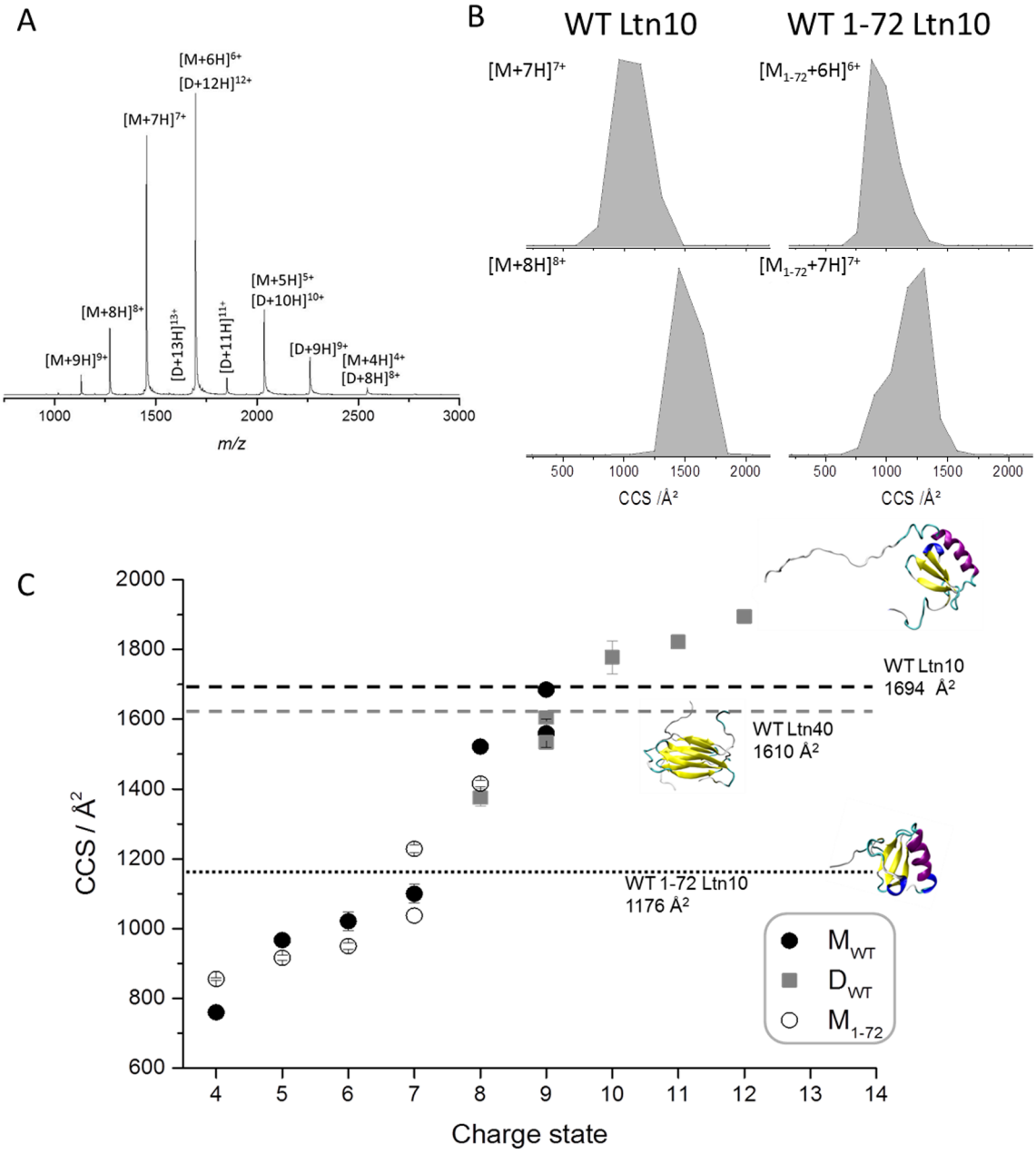

Figure 2. (A) WT Ltn spectra obtained in 20 mM ammonium acteate. (B) Collision cross section distributions derived from arrival time distributions at a drift voltage of 45 V, for monomeric WT Ltn $[M+7H]^{7+}$ and $[M+8H]^{8+}$ and WT 1−72 $[M_{1-72}+6H]^{6+}$ and $[M_{1-72}+7H]^{7+}$. (C) Experimentally determined CCS obtained for Ltn; average values obtained from three repeats for WT and WT 1−72 Ltn. WT monomer species are represented by black dots and WT dimer species by gray squares. Hollow circles represent the CCS determined for monomeric WT 1−72 Ltn. Dashed lines represent the theoretical CCS for the monomer and dimer calculated from PDB files 1J9O and 2JP1, respectively. The dotted line represents the theoretical CCS obtained for the clipped structure of the PDB file 1J9O, removing residues 73−93; corresponding representative structures are shown. In vacuo minimized structures from which theoretical CCS were obtained are shown here; structures prior to minimization are given in Figure 1.

analyzer. The instrument and its operation have been described in detail elsewhere.[44] All analyses were performed using 100 μM Ltn prepared in 20 mM ammonium acetate, pH 6.8. Each experiment was performed in triplicate, on separate days. Identical tuning conditions were employed for each sample: capillary voltage, 1.6 kV; cone voltage, 56 V; source temperature, 80 °C. The temperature and pressure of helium in the drift cell were approximately 28 °C and 4.0 Torr, respectively. Measurements were made at eight different drift voltages from 60 to 15 V.

Reference CCS from NMR Coordinates. As a starting reference, theoretical CCS from PDB file coordinates were calculated using the trajectory method of MOBCAL code.[45] Both NMR structures (PDB files 1J9O and 2JP1 for Ltn10 and Ltn40, respectively) plus the Ltn10 1−72 (obtained by clipping the disordered tail from the 1J9O structure) were minimized in vacuo using the *sander* engine of Amber12[46] and implementing the Amber99SB-ILDN force field.[47] In the minimization process, the first 5000 steps of the steepest descend algorithm were run, followed by as many steps of the conjugated gradient as sufficient to obtain a gradient convergence criterion (drms) equal to 0.005 kcal/mol·Å. For nonbonded interactions, an "infinite" radial cutoff (999 Å) was used. For Ltn40, as the 2JP1.pdb file contains 20 candidate models, each of these models was first in vacuo minimized, and their corresponding CCS were calculated, as

dx.doi.org/10.1021/jp504997k | J. Phys. Chem. B 2014, 118, 12348−12359

stated above. Subsequently, the average value for the 20 candidates was considered and reported as the theoretical CCS. The PDB file for WT Ltn contains an additional amino acid at its N-terminus (V) that is not present in the construct studied experimentally.

Solution- and Gas-Phase Molecular Dynamics Simulations. Insights into protein dynamics were achieved running molecular dynamics (MD) simulations for both Ltn10 and Ltn40 in explicit solvent and in vacuo; the simulation times were 150 ns for Ltn10 and 200 ns for Ltn40. For in vacuo simulations of Ltn10, the 7+ charge state was considered as this was the most abundant in MS and DT IM-MS and present in ECD studies. For Ltn40 in vacuo simulations, the 11+ charge state was considered as only the odd charge states of the dimer were studied by both DT IM-MS and ECD; furthermore, this dimeric charge state was observed at the highest intensity in the ECD studies. The modules *pmemd.cuda* and *sander* of the Amber12[46] suite of programs were utilized to propagate the trajectories in solution and in vacuo simulations, respectively. As for explicit solvent simulations, the electrostatic interactions were treated implementing the particle mesh Ewald (PME) with a radial cutoff of 8 Å; all of the bonds involving hydrogen atoms were constrained at their equilibrium distance, allowing an integration time step of 2 fs. As for the in vacuo simulations, electrostatics were treated via direct Coulomb summation with an "infinite" radial cutoff (999 Å), constraining all of the bonds involving hydrogen atoms at their equilibrium distance and using a time step of 1 fs. For all of the MD runs, the Amber99SB-ILDN force field[47] was utilized. A detailed explanation of the simulations settings is given in the Supporting Information together with a summary (Tables S4 and S8) of all of the types of runs carried out. The salt bridge occupancies were derived using the software *cpptraj*[48] of AmberTools13.[46] The command utilized was *hbond*, imposing a radial cutoff between the hydrogen bond donor and acceptor equal to 3 Å and disabling the angle cutoff (between the donor, hydrogen atom, and acceptor). The computation considered only the anionic carboxylate of acidic residues (Asp and Glu) and the cationic ammonium of basic residues (Lys and Arg). Occupancies of greater than 20% were reported in each case.

ECD. All high-resolution MS and ECD analyses were carried out on a 12 T Apex Qe FT-ICR (Bruker Daltonics). Analysis was carried out using ESI ionization of 5 μM Ltn in 100 mM ammonium acetate (for the monomer species) and with 30 μM Ltn in 100 mM ammonium acetate to transmit enough signal to perform ECD experiments on the dimers. Ion accumulation was in the range of 1−7 s, dependent on the intensity of the species. n-ESI was performed using a NanoMate (Advion biosciences) running in infusion mode and equipped with an HD_A_0 ESI chip (Advion biosciences). The ion accumulation time for all dimeric species was 10 s. In all cases, each spectrum was the sum of 300 acquisitions.

RESULTS

DT IM-MS of Ltn. In solution, Ltn exists in equilibrium between distinct monomer and dimer conformations.[4] The monomeric structure, Ltn10, adopts the conserved chemokine fold consisting of three β-sheet strands and an adjacent α-helix (Figure 1A).[49] The dimeric Ltn40 requires complete restructuring of the core residues[5] and consists of two identical units, each of which contains four β-sheet strands (Figure 1B), the three-dimensional structure of which is distinct from that of previously studied chemokine dimers.[50−52] Both Ltn10 and Ltn40 conformations contain an intrinsically disordered C-terminal tail. Under physiological solution conditions, both conformations are populated and interconvert rapidly. However, previous NMR studies have shown that it is possible to shift the equilibrium to favor one form or another through differing solution conditions.[4] The equilibrium of Ltn has also been previously studied using MS.[53]

We have established MS conditions that preserve both the monomer and dimer in a range of charge states indicative of solution conformations with different levels of proton accessibility (Figure 2A and Supporting Information Figures S1 and S2). The more structured/compact a given conformation is, the fewer available sites there will be for protonation. The monomer (M) is the more populated species, presenting over a charge state range from $[M+4H]^{4+}$ to $[M+9H]^{9+}$, with $[M+7H]^{7+}$ and $[M+6H]^{6+}$ ions at the highest intensities (Figure 2A). The dimer (D) is present at a lower intensity and over a charge state range from $[D+8H]^{8+}$ to $[D+13H]^{13+}$; charge states of the dimer that have an even net charge are m/z coincident with monomeric species possessing half of the net charge (Figure 2A). For the WT 1−72 construct, the monomer was present over the charge state range $[M_{1-72}+4H]^{4+}$ to $[M_{1-72}+8H]^{8+}$. Although a small proportion of dimer was also observed due to its low intensity, analysis of WT 1−72 focused on the monomeric species (Supporting Information Figure S3A). To explore conformations presented by Ltn in both its monomeric and dimeric form, we utilized DT IM-MS, where ATDs (Figure 2B) for each m/z selected ion can be obtained as described above.

DT IM-MS of Full-Length 1−93 and Truncated 1−72 Monomeric Ltn10. CCS have been determined for monomeric Ltn over the charge state range of $[M+4H]^{4+}$ to $[M+9H]^{9+}$ and for 1−72 Ltn over the charge state range of $[M_{1-72}+4H]^{4+}$ to $[M_{1-72}+8H]^{8+}$ (Figure 2C and Supporting Information Tables S1 and S2). For both monomers (full length and 1−72), as the charge increases, the CCS increases, attributed to increased access to protonatable sites in solution for the more unfolded forms, in turn providing larger CCS values. In the gas phase, Coulombic repulsion between proximal charged groups in partially unfolded forms will contribute to the increase of CCS with charge. For the full-length monomer, the lowest charged species observed is $[M+4H]^{4+}$, present at low intensity with a CCS significantly smaller than that of the $[M+5H]^{5+}$; this has been attributed to a significant collapse, as has been reported previously for monomeric proteins.[23,31,54]

Interestingly, the most significantly populated species $[M+5H]^{5+}$ to $[M+7H]^{7+}$ all present similar CCS, around 1000 Å^2. This suggests that there is a compact, stable structural ensemble in solution that is able to accept between 5 and 7 net protons, without a major unfolding transition. The slight CCS increase over this charge state range is attributable to Coulombic effects, as described above, and is similar to observations made for the monomeric structurally constrained construct of Ltn10.[55] The 1−72 truncated form presents very similar CCS to the full length over the charge state range of 5−7+ although typically smaller by a factor of ∼6%; a second more extended conformation, however, is also observed for $[M_{1-72}+7H]^{7+}$ and discussed below. Interestingly, the 4+ ion, which is also weak for the truncated form (Supporting Information Figure S3), possesses a somewhat larger CCS by 12% than that found for the full-length monomer.

For the full-length monomer, a significant increase (up to 42% compared with $[M+7H]^{7+}$) in CCS is observed for the $[M+8H]^{8+}$ and $[M+9H]^{9+}$ ions, suggesting that a major unfolding event has occurred, as clearly seen in the shift in ATD (Figure

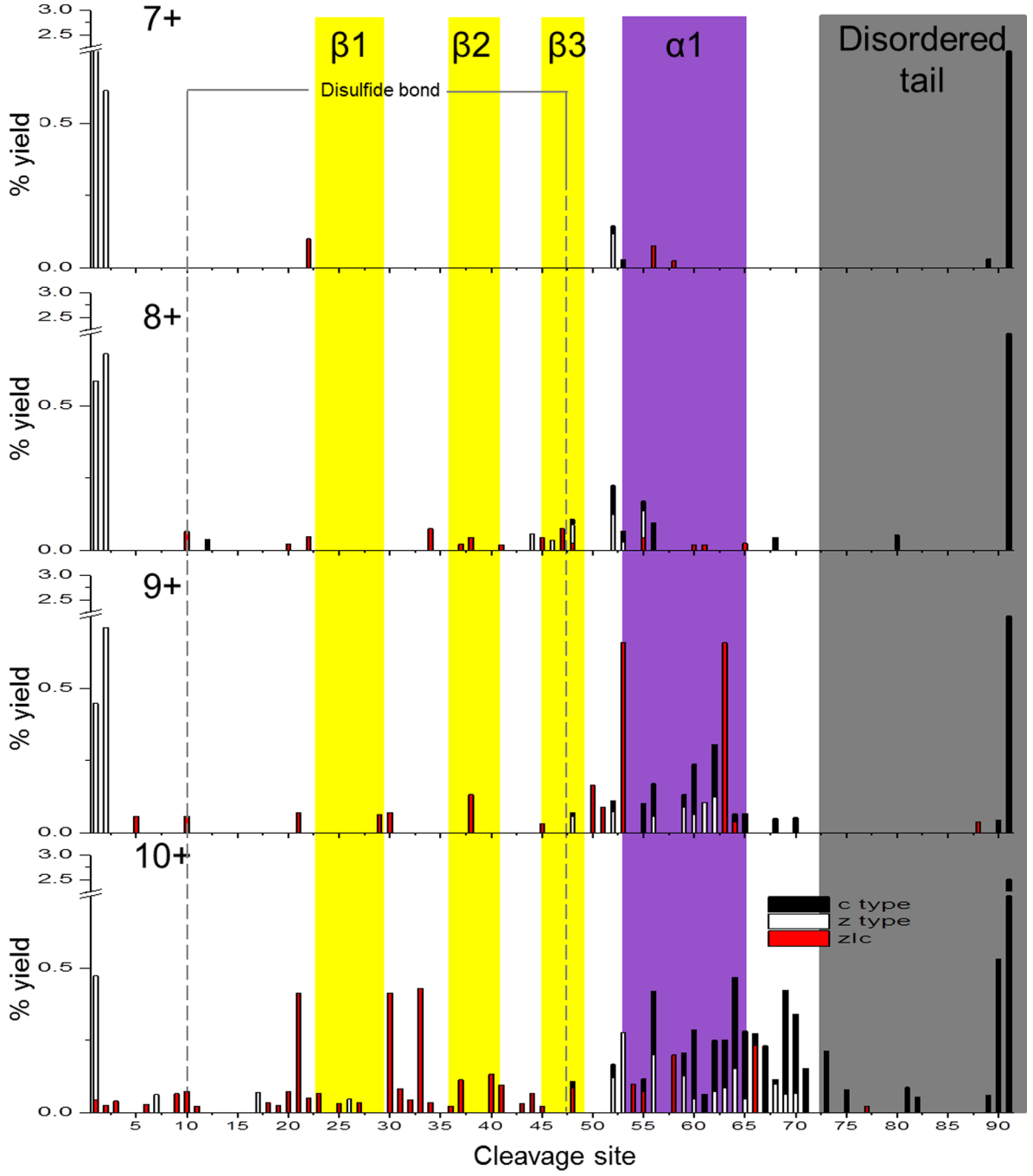

Figure 3. Percentage yields calculated for c-type, z-type, and zIc fragments as a function of cleavage site for monomeric Ltn over the charge states $[M+7H]^{7+}$ to $[M+10H]^{10+}$. Each zIc fragment has a pair of cleavage sites (see Figure 4). A *y*-axis scale break is present for all charge states to show low-level fragmentation more clearly.

2B). A second even more extended conformation is also observed for the $[M+9H]^{9+}$ charge state, which has been assigned to a conformer further along the unfolding pathway. The truncated 1−72 form also has an increase in CCS, although here it is between the $[M_{1-72}+6H]^{6+}$ and $[M_{1-72}+7H]^{7+}$ ions. The shift in CCS is less for the 1−72 Ltn10 and proceeds via two intermediates for the $[M_{1-72}+7H]^{7+}$ ion (Figure 2B).

Comparison between the experimental CCS and predicted CCS from NMR coordinates (PDB file 1J9O) shows that for the full-length monomer, all gas-phase conformations are smaller than the predicted value (1694 Å^2), although the highest charge states are comparable to the CCS calculated from the NMR structure. The PDB monomer structure 1J9O contains the intrinsically disordered tail extended from the structural core of the protein, resulting in a large theoretical CCS. Another theoretical CCS was determined by clipping the NMR structure (PDB 1J9O), removing residues 73−93, and leaving the N-terminus and the structural core of the protein.

When the tail is removed from the structure, a theoretical CCS of 1176 Å^2 is obtained, which is in agreement with the experimental CCS determined for full-length Ltn10 in the charge state range of $[M+5H]^{5+}$ to $[M+7H]^{7+}$, however, slightly larger than these experimental values (∼7% larger with respect to $[M+7H]^{7+}$). This theoretical value also agrees with the

dx.doi.org/10.1021/jp504997k | J. Phys. Chem. B 2014, 118, 12348−12359

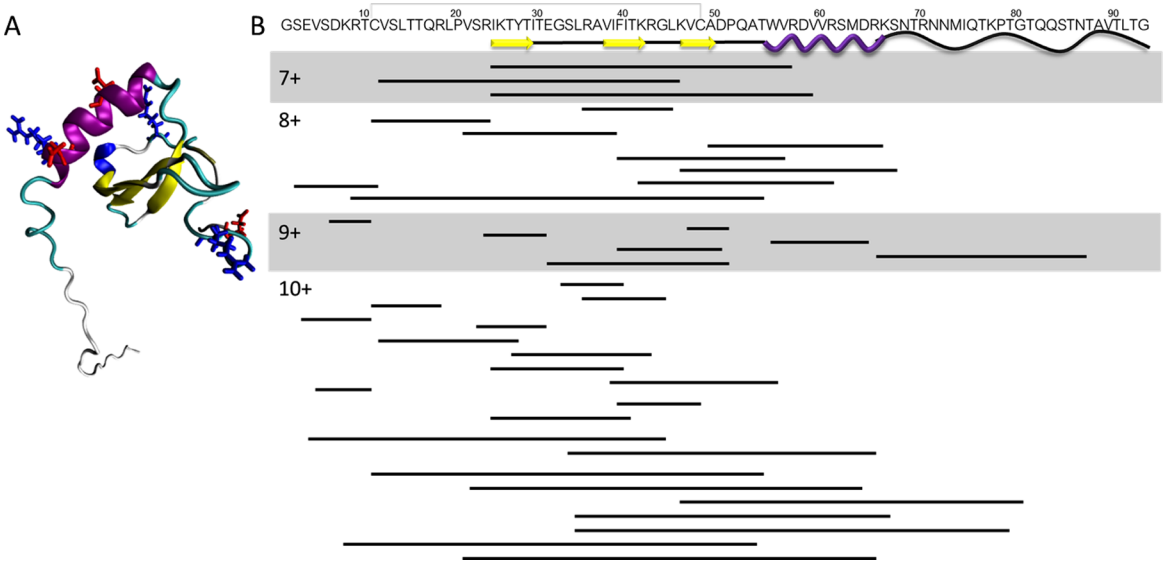

Figure 4. (A) WT Ltn (PDB 1J9O) with labeled residues for all potential salt bridges with acidic residues in red and basic in blue. B) zIc fragmentation map for monomeric WT Ltn. The position of the disulfide bond is shown with a solid grey line. Solid black lines indicate zIc fragments for each charge state.

experimental values obtained for the 1−72 truncated form, suggesting that for the full length Ltn, at the most populated charge states of 7+ and below, the C-terminal tail is associated with the core. We checked the likelihood of the tail associating with the protein core under these experimental conditions by performing an analysis of the WT 1−72 form mixed with the tail peptide (72−93). Under equimolar conditions, a noncovalent complex is observed in charge states 4+ to 7+ (Supporting Information Figure S3).

Given that the truncated form and the theoretical value of the truncated form agree with the experimental CCS values for the full length Ltn10 at low charge states, the larger CCS for ions $[M+8H]^{8+}$ and $[M+9H]^{9+}$ may be attributed to conformers wherein the intrinsically disordered tail is no longer fully associated with the protein core, as for solution. This is supported by the strong correlation between these CCS values and the theoretical value obtained from full length 1J9O. The remainder of the analysis of Ltn will focus on the full-length forms.

DT IM-MS for Dimeric Ltn, Ltn40. The same DT IM-MS experiments on WT Ltn provide data for the dimeric Ltn40 form. The experimental CCS adopted over the charge states $[D+8H]^{8+}$ to $[D+13H]^{13+}$ were determined (Figure 2C and Supporting Information Table S3). $[D+11H]^{11+}$ and $[D+13H]^{13+}$ ions have similar CCS of around 1800−1900 Å^2, in good agreement but marginally larger than the predicted CCS from the NMR coordinates. The theoretical CCS obtained from the 20 candidate structures lie over a range (1550−1700 Å^2) with an average value of 1610 Å^2, varying due to the position of their termini. However, the PDB file (2JP1) used to predict the CCS does not contain the full disordered C-termini, which would explain the slightly smaller predicted size. The difference between the experimental full sequence protein and predicted value, omitting 33 amino acids (from each chain), is relatively small, and we surmise that the (here longer) tail is again associated with the structural core and starting to unfold as the charge state increases. The CCS for $[D+8H]^{8+}$ and $[D+9H]^{9+}$, however, are smaller (up to 29% smaller than $[D+10H]^{10+}$) than the other dimer charge states and up to 15% smaller than the predicted CCS. Their smaller size in comparison to the stable conformational family presented over the charge state range of $[D+10H]^{10+}$ to $[D+13H]^{13+}$ suggests that these species are most likely a product of "gas-phase collapse" or a less structured solution-phase encounter complex between the unfolded monomeric chains. Additionally, two conformations are observed for the $[D+9H]^{9+}$ species, suggesting that this may be a transition species between a collapsed and structurally more stable form.

ECD of Monomeric Ltn, Ltn10. Each observed charge state of both the monomer and dimer can be individually probed using ECD. The average charge state is higher in the ECD experiments as compared to those found for DT IM-MS analysis, for the both monomer and dimer, which we attribute to differences in the instrumentation being utilized (Supporting Information Figure S4). For analysis of Ltn10, the charge states $[M+7H]^{7+}$ to $[M+10H]^{10+}$ were observed at high enough intensity for effective trapping and with sufficient fragmentation efficiency for analysis by ECD (Supporting Information Figure S5). The percentage yield of all observed c, z, and internal fragments as a function of cleavage site are shown mapped onto the Ltn10 fold in Figure 3; b- and y-type fragments were also considered; however, here, their influence was negligible and hence will not be discussed further. For both the monomer and dimer, we see internal fragments formed via fragmentation at both the N- and C-terminus, which, because, they contain a z-type fragment at their N-terminus and a c-type fragment at their C-terminus, we denote as "zIc" fragments where "I" refers to the fact they are internal, following the nomenclature developed by Roepstorff and Fohlman.[56]

As the charge state increases, an increase both in the extent of fragmentation occurring along the backbone and in the fragment ions' percentage yield is observed. The efficiency of ECD is higher at higher charge states,[57] but in addition, we can attribute observed fragments to the absence of stabilizing noncovalent interactions that would be present in the solution fold (Figure 3). For charge states 7+ and 8+, we see very little fragmentation from residues 54−66, which in solution form an α-helix, whereas for 9+ and 10+, significant fragmentation occurs in this region, as well as in the N-terminus. These high charge states, therefore, are

dx.doi.org/10.1021/jp504997k | J. Phys. Chem. B 2014, 118, 12348−12359

attributed to a form of Ltn10 where unfolding has led to protonatable sites being accessed. Interestingly, for the ions $[M+8H]^{8+}$ to $[M+10H]^{10+}$, the intrinsically disordered C-terminal tail can be lost in its entirety, for which c-type fragments are observed for charge states 8+ and 9+ in the region between the α-helix and ID tail, with the complementary z-type fragments also being observed for the 10+ charge state. This cleavage occurs in the region between the α-helix and the start of the disordered tail (residues 67−72), and when fragmentation occurs here, loss of the entire C-terminus suggests that there is no longer any association with the core, entirely consistent with the ion mobility data above. At the 10+ charge state, there is a rise in fragmentation along the C-terminal tail and also along the N-terminus, suggesting a reordering event enabling the tail itself to fragment.

Consideration of Stabilizing Interactions: the Role of the Disulfide Bond and Salt Bridges. At all charge states, when fragmentation occurs within the regions that are β-sheet in solution, the fragment ions are of lower intensity than those resulting from fragmentation at either termini or the α-helix. Indeed, even at the highest charge state, in which we see the most extensive fragmentation across the protein, only 25% of the total fragments observed occurred due to fragmentation in this region, corresponding to 17% of the overall summed intensity of all observed fragments. Furthermore, when cleavage in this region occurs, it results in zIc fragments generally consisting of more than one β-strand, suggesting that the fragments at least partially retain some of the stabilizing interactions present in the solution fold (Figure 4). We speculate that zIc fragments are particularly prevalent following ECD of β-sheet-rich proteins. We have further studied the β-sheet-rich protein β2-microglobulin with ECD (Supporting Information Figures S6 and S7) and find a similar pattern; very little c- or z-type fragmentation is observed in contrast to a higher proportion of zIc fragmentation. Previous reports of internal fragments have suggested that these species can be formed via charge remote fragmentation in peptides that contain basic residues in the middle of the sequence;[58] hence, the high proportion of internal fragments observed here could be due to the highly basic nature of this protein.

When considering whether the data for any given charge state suggests preservation or loss of either global fold or secondary structural elements in the gas phase, it is instructive to consider what interactions could stabilize the fold. The disulfide bridge between residues 10 and 47 covalently bonds these regions, and we observe several fragments with this bridge intact (Figures 3 and 4). We also see disulfide reduced fragments (which increase in intensity with charge state), suggesting that this bond becomes more accessible to electron capture, which indicates unfolding of the protein with charge state, as found by DT IM-MS above. In the gas phase, salt bridges can provide strengthening interactions to preserve solution fold. In order to probe the possibility of salt bridge retention or formation in the gas phase, MD simulations were performed (see Supporting Information section S5 and Table S4). First, two separate 150 ns MD trajectories were run in explicit solvent to identify the potential salt bridges in solution, which are shown in Supporting Information Tables S5 and S6. An occupancy cutoff of 20% was applied to identify the most likely salt bridges, and pooling the two simulations resulted in the identification of the following interactions: Glu3-Arg8, Asp6-Arg8, Glu30-Arg56, Asp57-Arg17, and Asp57-Arg60. In the solvent-free environment of the gas phase, electrostatic interactions strengthen, and this had the potential to tighten any of these salt bridges and even form new interactions. Gas-phase MD simulations were run on the $[M+7H]^{7+}$; charge states 5−7+ were observed to be the most intense in MS and DT IM-MS studies; hence, these three charge states are the most desirable targets for MD simulations. However, due to the harsher desolvation conditions of the FT ICR-MS instrument, only charge states 7−10+ could be observed at high enough intensity to be subjected to ECD. Therefore, the 7+ charge state was chosen for further study (see the Supporting Information and Figure S8 for details). The MD simulations show that the salt bridges between Glu3-Arg8, Asp57-Arg17, and Asp57-Arg64 all increase in occupancy in the gas phase, and an additional salt bridge is formed between Asp63-Arg60 (Supporting Information Table S7). Both the Asp57-Arg60 and Asp63-Arg60 can act to stabilize the α-helix, while the Asp57-Arg17 would help position the α-helix within the structural core (Figure 4). These simulations also provide evidence for the intrinsically disordered tail folding in toward the structural core in solution (Supporting Information Figures S9 and S10), which remains associated in the gas phase, resulting in a compact CCS of ∼1250 Å^2 (Supporting Information Figure S11), providing further support to our interpretation of the DT IM-MS data.

For the lower charge states (7 and 8+), in the region of 3−91, little fragmentation is observed, consistent with a compact structured conformational family stabilized by noncovalent interactions, as well as the disulfide bridge. An exception to this is at the two termini where fairly high losses are observed and also at Ala52 in the loop between the end of the triple strand β-sheet and the start of the α-helix, causing the loss of residues 54−91 in a single z-type fragment, suggesting that the α-helix is separable from the β-strand core and that the salt bridge between Asp57-Arg60 and Arg60-Asp63 can provide intrahelix stabilization, enabling it to be lost in a single fragment. The loss of the α-helix is at a relatively low intensity, and this may be due to the (lesser occupied) salt bridge between β1 and α-helix (Asp57-Arg17), which would limit α-helix dissociation.

Visual examination of the PDB file 1J9O identifies an additional potential "classical" salt bridge comprising Glu30-Arg34 and Arg34-Asp49. MD simulations for Ltn10 in water suggest that these interactions can occur (Supporting Information Figure S12) although at lower occupancy than those listed in Supporting Information Tables S5 and S6. This bridge strengthens significantly within the gas phase (Supporting Information Figure S13). This classical salt bridge motif is positioned across the top of the triple stranded β-sheet and if present could (in combination with the disulfide bond) provide an intriguing explanation for the gas-phase stability of that region.

Comparing the gas-phase studies to those carried out previously in solution using NMR[43] can provide further information. For $[M+7H]^{7+}$, there is a zIc fragment observed due to the preservation of residues 24−56 and the corresponding loss of residues 1−23 (arising with disulfide bridge cleavage) and 57−91 suggesting that both termini are detachable. NMR studies on Ltn10 found that residues 1−10 have less NOE restraints and higher RMSD values, corresponding to a dynamic N-terminal region, in which we observe extensive backbone fragmentation, even in low charge states. By contrast, residues 11−23 are more ordered, with long-range NOEs and backbone RMSDs below 0.5 Å in part attributed to the disulfide bond,[43] and we observe less fragmentation here.

When considering the $[M+9H]^{9+}$ species, it is important to note that in the DT IM-MS experiments, two conformations are observed. The more extended of these has a CCS of 1685 Å^2 and corresponds to a highly extended conformer. Fragments arising

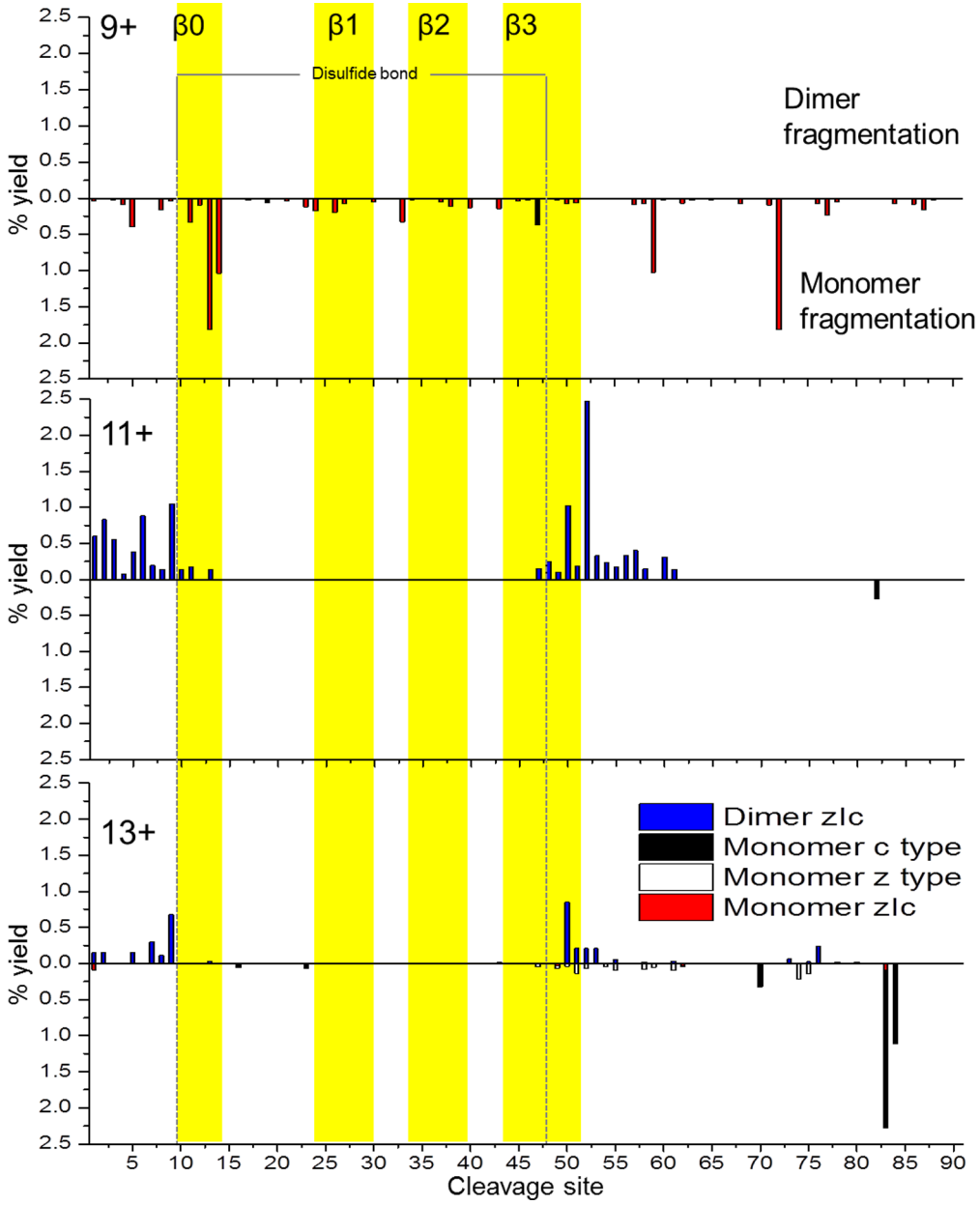

Figure 5. Percentage yields calculated for c-type, z-type, and zIc fragments as a function of cleavage site for dimeric Ltn over the charge states $[D+9H]^{9+}$, $[D+11H]^{11+}$, and $[D+13H]^{13+}$. Above-axis histograms represent fragments formed while retaining the dimer interface. Below-axis histograms represent fragments formed following dimer dissociation to monomer.

from $[M+9H]^{9+}$ show extensive fragmentation in residues 45–65, demonstrating that β3 and α1 are here unravelled from the structural core, suggesting a loss of the influence of the Asp57-Arg17 and the intrahelix (Asp57-Arg60 and Asp63-Arg60) interactions, allowing cleavage to be accompanied by dissociation. In contrast, residues 23–28 (β1) and 36–40 (β2) remain relatively unperturbed (Figures 3 and 4). Significant fragmentation in the β1 and β2 part of the core protein only occurs for $[M+10H]^{10+}$. At this charge state, more extensive fragmentation occurs along the backbone, resulting in the formation of internal, c-, and z-type fragments, most likely as a result of both the higher charge state, promoting more efficient fragmentation, and increased unfolding of the higher charged ions.

ECD of Dimeric Ltn, Ltn40. To probe Ltn40, we considered dimeric ions carrying an odd net charge and therefore not coincident with monomer species, namely, $[D+9H]^{9+}$, $[D+11H]^{11+}$ and $[D+13H]^{13+}$. As for the monomer, c-type, z-type, and zIc summed fragment yields were analyzed; however, because both monomeric units are identical in sequence, these experiments do not distinguish between the two chains, and therefore, the total fragment percentage yields are mapped onto a single monomeric unit (Figure 5).

All fragments from the $[D+9H]^{9+}$ dimer are smaller than a single monomer and correspond to zIc fragments distributed all along the polypeptide backbone, which suggests that the intermolecular interactions are not strong. The instability of the dimer at this charge state can be attributed to collapse upon ionization and transfer. Another possibility is that it is a less structured form present in solution. Assigning this as a partially collapsed form is consistent with findings from DT IM-MS where the CCS for the lowest charge states observed following n-ESI from buffered conditions are consistently lower than that

dx.doi.org/10.1021/jp504997k | J. Phys. Chem. B 2014, 118, 12348–12359

Figure 6. (A) Ltn40 (PDB 2JP1) with putative interchain salt bridges labeled; acidic residues are shown in red and basic in blue. (B) All stretches of internal fragments observed in one or more zIc fragments for the $[D+11H]^{11+}$ and $[D+13H]^{13+}$ species, the summed intensity of which is shown in Figure 5. The disulfide bond is highlighted on the sequence by the solid line.

found from PDB coordinates of solution structures,[31] an observation that has been made since the earliest use of IM-MS to examine proteins.[23]

At the two higher charge states studied, the dimer is more stable, characterized by a decrease in dissociation to monomer and substantially less backbone fragmentation with almost complete retention of the dimeric interface residues 11−51. There is minimal fragmentation in the β-sheet core, with the majority of fragments arising from cleavage on either side of this structural core, residues 1−10 and 47−61, suggesting that the core remains stable and perhaps preserved in the gas phase, highlighting the particular stability of the Ltn40 β-sheet region. At high protein concentrations, oligomers can be formed during the electrospray process;[59] however, the DT IM-MS and ECD results suggest that here the higher charge states of the dimeric protein are specific complexes, which retain solution-phase topologies.

Consideration of Stabilizing Interactions: The Role of the Disulfide Bonds and Salt Bridges. As with the monomer species, it is important to consider possible interactions that could serve to stabilize the Ltn40 β-sheet core within the gas phase in order to better understand the enhanced stability of the intermolecular interactions in both the $[D+11H]^{11+}$ and $[D+13H]^{13+}$ species. As with Ltn10, MD simulations were performed in solution and in vacuo to identify any potential salt bridges, which if present would act to stabilize the gas-phase structure (Supporting Information Table S8). The potential identified salt bridges and their occupancies can be found in Supporting Information Tables S9 and S10 (for the two in solution runs) and Table S11 (for the in vacuo run). The gas-phase simulations performed on $[D+11H]^{11+}$ identified a number of intrachain salt bridges between residues Asp49-Arg8 and Asp49-Arg34 for chain A and interactions between Asp6-Lys7, Asp49-Arg8, Asp49-Arg34, and Asp57-Arg56 for chain B; the increase in salt bridges for chain B in comparison with those for chain A is most likely due to an asymmetric distribution of charges in the 11+ species because chain A contains an additional charge (Supporting Information Figure S15). All of the identified intrachain salt bridges lie on the edges of the β-sheet core, and hence, if these interactions are preserved in the gas phase, they would stabilize this structural region. Furthermore, the disulfide bond is present in Ltn40 and will provide intrachain stability. Significantly, a high number of possible interchain salt bridges was identified, Arg22-Glu30, Glu30-Lys24, Arg22-Asp57, Asp57-Arg17, Arg42-Glu3, Arg17-Glu3, Glu30-Arg61, and Glu30-Arg22 (denoted chain A-chain B). All of these putative salt bridges lie on the edges of the β-strands and if present would strengthen the dimer interface (Figure 6A). The presence of these interactions and their stabilizing influence are supported by the fact that these salt bridge forming residues are regularly retained in zIc fragments, (see Figure 6). The calculated CCS of the $[D+11H]^{11+}$ as a function of time during the 200 ns production run centered on ∼1590 Å^2, smaller than the experimental value (1802 Å^2) for this species as determined by DT IM-MS; however, the differences here can be attributed to the C-terminal tail, which was not present in the starting structure used for MD simulations (PDB 2JP1), and will certainly increase the CCS.

DISCUSSION

The metamorphic protein Ltn presents us with the opportunity to study a highly dynamic protein and the conformations that can be sampled using MS. Charge state distributions, and CCS report on the (known) structural heterogeneity of this protein in solution; this is also shown by the distinct fragmentation patterns obtained for distinct charge states. Comparison of ECD fragmentation maps for monomeric and dimeric Ltn (Figures 3 and 5) show striking differences between the two, and within each, there are notable trends as the charge states increases, providing evidence for dynamics in both Ltn10 and Ltn40 conformations in the absence of solvent and the power of this technique to report on metamorphic systems.

First, considering residues 10−25 in Ltn10, this region has little structure, and we observe fragmentation along the backbone. However, in Ltn40, these residues form the β0 strand and subsequent loop to β1; we find very little fragmentation in this region, which has increased structural stability in Ltn40 compared to that in Ltn10. We ascribe this higher stability of the dimer to a higher number of potential (intra- and interchain) salt bridges involving residues 10−25, identified using MD simulations. Second, for residues 54−66, in Ltn10, these residues comprise the α-helical region, and ECD fragmentation of the higher charge states shows cleavage along the entire backbone in this region, consistent with unravelling of an α-helical region. In contrast, for Ltn40 (in 11+ and 13+ charge states), we do not see the same fragmentation along this region; instead, fragmentation is observed to branch out from the structural β-sheet core. Indeed, the most favorable fragmentation site is observed to be

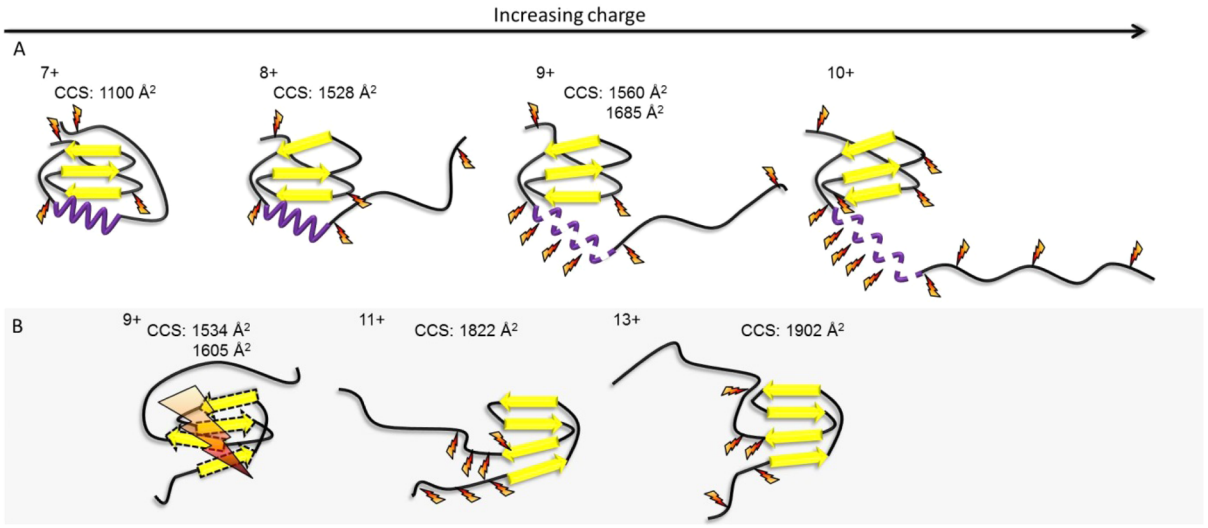

Figure 7. A cartoon representation of the conformers observed for (A) Ltn10 over the charge states $[M+7H]^{7+}$ to $[M+10H]^{10+}$ and (B) Ltn40 for charge states $[D+9H]^{9+}$, $[D+11H]^{11+}$, and $[D+13H]^{13+}$. Orange "lightning bolts" indicate sites where ECD fragmentation is most significant. For $[D+11H]^{11+}$ and $[D+13H]^{13+}$, the dimer is represented here by a single monomeric unit. For $[D+9H]^{9+}$, where fragments only map to a monomer unit with no secondary structure, the extensive fragmentation is depicted by a large lightning bolt, and dashed lines represent a lack of defined structural elements.

residue 52, showing that the loss of residues 52−93, which contain little secondary structure in Ltn40 while retaining the structural core, is preferential. This finding is consistent with the lower number of salt bridges (in comparison to residues 10−25) identified through MD simulations, which could stabilize this region with respect to the core of the dimer. Additionally, we obtain more fragmentation in the nine amino acids that form the first part of the disordered tail (residues 52−60), which suggests that this region is somewhat associated with the protein core, facilitating the ECD mechanism, and indeed, this is the case in solution because NMR analysis allowed this region to be solved (Figure 1B). These significant differences in the ECD fragmentation of two WT Ltn species, in combination with the results from DT IM-MS, suggest the distinct folds of this metamorphic protein can be preserved in an unsolvated form.

Through the combination of ECD, DT IM-MS, and MD simulations, we can build up a detailed picture of the metamorphic nature of this protein. Lower charge states of Ltn10 are compact and give CCS much less than the NMR structure, in which the C-terminus is extended; the increase in CCS from $[M+8H]^{8+}$ could be attributed to the intrinsically disordered tail unfolding from the structural core. This is supported by MD of the $[M+7H]^{7+}$ form, where the disordered tail is found to associate with the protein, and by experiments on the truncated form of Ltn10. An increase in ECD fragmentation between the $[M+7H]^{7+}$ and the $[M+8H]^{8+}$ ions provides further evidence for this and suggests that the tail stabilizes the protein when more tightly associated. The lack of fragments from within the disordered tail suggests that the tail has some structural stability; it departs as a single long peptide once cleaved at Asn67. For $[M+10H]^{10+}$, fragmentation within the α-helical section and now in the disordered tail indicates that the disruption of the tail's association with the proteins starts to disrupt the α-helix (or vice versa) and that there is significant rearrangement across these charge states of the C-terminal region. The β-sheet core in this more extended species still remains relatively unperturbed, providing a ranking order for the stability of the regions comprising the Ltn10 fold: C-terminus < N-terminus < α-helix < β-sheet core. By considering CCS in combination with the cleavage sites and fragmentation of the monomer over all charge states, we gain insights into the fold stability as a function of increased charge, which is depicted in Figure 7A.

For the dimeric form of Ltn, Ltn40, we examine conformations adopted over three charge states. DT IM-MS results show a compaction for the lowest charge state, $[D+9H]^{9+}$ (as seen for the lowest charge state of the monomer $[M+4H]^{4+}$), which corresponds to a structurally less stable dimer conformation, which undergoes extensive dissociation to monomer fragments with no relation to structured core regions. However, for the remaining two charge states, $[D+11H]^{11+}$ and $[D+13H]^{13+}$, both techniques reveal stable conformations that map extremely well to the solution structure. The results suggest that the intrinsically disordered tail is wrapped around the structural core of the protein and that the less dynamic part of this tail (residues 52−60) is more closely associated. In addition, comparison of DT IM-MS results with molecular modeling and ECD fragmentation maps suggest that the β-sheet core of the protein remains intact and structurally stable; these findings are summarized in Figure 7B.

SUMMARY

In summary, for the metamorphic protein lymphotactin, in both its monomeric and dimeric forms, the solution fold can be preserved in the gas phase, allowing the structural plasticity of this protein to be studied. Significantly, for Ltn10, a number of conformations are observed that correspond to a collapsed form, a conformational family in which the intrinsically disordered tail is associated with the core, as well as an extended conformational family attributed to undocking of the tail. In both Ltn10 and Ltn40, there is evidence for stability within the β-sheet regions of the solution fold in the gas phase, which we find more stable than the α-helix and both termini. It is interesting to speculate that the stability within these regions in Ltn may be due to preservation of charged β-sheets in the gas phase, presenting Ltn as an interesting target for future gas phase studies to definitively determine if β-sheets can be preserved in a solvent-free environment within protein ions. Further studies of Ltn mutants[55] will allow the stabilities of mutant folds to be

dx.doi.org/10.1021/jp504997k | J. Phys. Chem. B 2014, 118, 12348−12359

compared to WT and may help in the design of future forms designed to mimic one of the distinct conformations. Our findings highlight that MS, DT IM-MS, MD, and ECD can be used to probe highly dynamic protein systems, elucidating species occurring along the unfolding pathway and providing insight into the conformations adopted in a solvent-free environment. The combination of these techniques has provided unique insights into the relationship between structure and dynamics of this metamorphic protein, which will be applicable more widely to other conformationally dynamic proteins.

■ ASSOCIATED CONTENT

Supporting Information

Further experimental details for the drift tube ion mobility mass spectrometry experiments, tables of experimental collision cross sections obtained from DT IM-MS experiments, spectra obtained, and further information on the ECD fragmentation experiments are provided. In addition experimental details and results from molecular dynamics simulations are also provided. This material is available free of charge via the Internet at http://pubs.acs.org.

■ AUTHOR INFORMATION

Corresponding Author

*E-mail: perdita.barran@manchester.ac.uk.

Notes

The authors declare no competing financial interest.

■ ACKNOWLEDGMENTS

The Schools of Chemistry and Physics at the University of Edinburgh are thanked for an award of an EPSRC DTA studentship to S.R.H and for their continuing support of our research. Dr. Logan Mackay is thanked for assistance with FT-ICR MS and Dr. Adam Stokes for fabrication of 3-D models of lymphotactin (see the graphical abstract). Dr. Dominic Campopiano is thanked for his insights into protein expression. Dr. Michel Laguerre (Institut Européen de Chimie et Biologie (IECB), Pessac, France) is thanked for providing access to computational resources. We are grateful to Dr. Martin De Cecco for providing the initial inspiration to study Ltn.

■ REFERENCES

(1) Levinthal, C. How to Fold Graciously. In *Mössbauer Spectroscopy in Biological Systems Proceedings*; University of Illinois: Urbana, IL; 1969; pp 22−24.

(2) Kelner, G.; Kennedy, J.; Bacon, K.; Kleyensteuber, S.; Largaespada, D.; Jenkins, N.; Copeland, N.; Bazan, J.; Moore, K.; Schall, T. Lymphotactin: A Cytokine That Represents a New Class of Chemokine. *Science* **1994**, *266*, 1395−1399.

(3) Rossi, D.; Zlotnik, A. The Biology of Chemokines and Their Receptors. *Annu. Rev. Immunol.* **2000**, *18*, 217−242.

(4) Tuinstra, R. L.; Peterson, F. C.; Kutlesa, S.; Elgin, E. S.; Kron, M. A.; Volkman, B. F. Interconversion between Two Unrelated Protein Folds in the Lymphotactin Native State. *Proc. Natl. Acad. Sci. U.S.A.* **2008**, *105*, 5057−5062.

(5) Tyler, R. C.; Murray, N. J.; Peterson, F. C.; Volkman, B. F. Native-State Interconversion of a Metamorphic Protein Requires Global Unfolding. *Biochemistry* **2011**, *50*, 7077−7079.

(6) Fenn, J.; Mann, M.; Meng, C.; Wong, S.; Whitehouse, C. Electrospray Ionization for Mass Spectrometry of Large BiomoleculeS. *Science* **1989**, *246*, 64−71.

(7) Wilm, M. S.; Mann, M. Electrospray and Taylor-Cone Theory, Dole's Beam of Macromolecules at Last? *Int. J. Mass Spectrom. Ion Process.* **1994**, *136*, 167−180.

(8) Benesch, J. L. P.; Ruotolo, B.; Simmons, D. A.; Robinson, C. V. Protein Complexes in the Gas Phase Technology for Structural Genomics and Proteomics. *Chem. Rev.* **2007**, *107*, 3544−3567.

(9) Heck, A. J. R. Native Mass Spectrometry: A Bridge between Interactomics and Structural Biology. *Nat. Methods* **2008**, *5*, 927−933.

(10) Patriksson, A.; Marklund, E.; van der Spoel, D. Protein Structures under Electrospray Conditions. *Biochemistry* **2007**, *46*, 933−945.

(11) Meyer, T.; de la Cruz, X.; Orozco, M. An Atomistic View to the Gas Phase Proteome. *Structure* **2009**, *17*, 88−95.

(12) Stearns, J. A.; Boyarkin, O. V.; Rizzo, T. R. Spectroscopic Signatures of Gas-Phase Helices: Ac-Phe-$(Ala)_5$-Lys-H^+ And Ac-Phe-$(Ala)_{10}$-Lys-H^+. *J. Am. Chem. Soc.* **2007**, *129*, 13820−13821.

(13) Boyarkin, O. V.; Mercier, S. R.; Kamariotis, A.; Rizzo, T. R. Electronic Spectroscopy of Cold, Protonated Tryptophan and Tyrosine. *J. Am. Chem. Soc.* **2006**, *128*, 2816−2817.

(14) Stearns, J. A.; Seaiby, C.; Boyarkin, O. V.; Rizzo, T. R. Spectroscopy and Conformational Preferences of Gas-Phase Helices. *Phys. Chem. Chem. Phys.* **2009**, *11*, 125−132.

(15) Pagel, K.; Kupser, P.; Bierau, F.; Polfer, N. C.; Steill, J. D.; Oomens, J.; Meijer, G.; Koksch, B.; von Helden, G. Gas-Phase IR Spectra of Intact α-Helical Coiled Coil Protein Complexes. *Int. J. Mass Spectrom.* **2009**, *283*, 161−168.

(16) Dugourd, P.; Antoine, R.; Breaux, G.; Broyer, M.; Jarrold, M. F. Entropic Stabilization of Isolated β-Sheets. *J. Am. Chem. Soc.* **2005**, *127*, 4675−4679.

(17) Ruotolo, B.; Tate, C. C.; Russell, D. H. Ion Mobility-Mass Spectrometry Applied to Cyclic Peptide Analysis: Conformational Preferences of Gramicidin S and Linear Analogs in the Gas Phase. *J. Am. Soc. Mass Spectrom.* **2004**, *15*, 870−878.

(18) Bernstein, S. L.; Liu, D.; Wyttenbach, T.; Bowers, M. T.; Lee, J. C.; Gray, H. B.; Winkler, J. R. α-Synuclein: Stable Compact and Extended Monomeric Structures and pH Dependence of Dimer Formation. *J. Am. Soc. Mass Spectrom.* **2004**, *15*, 1435−1443.

(19) Frimpong, A. K.; Abzalimov, R. R.; Uversky, V. N.; Kaltashov, I. A. Characterization of Intrinsically Disordered Proteins with Electrospray Ionization Mass Spectrometry: Conformational Heterogeneity of α-Synuclein. *Proteins: Struct., Funct., Bioinf.* **2010**, *78*, 714−722.

(20) Keppel, T. R.; Howard, B. A.; Weis, D. D. Mapping Unstructured Regions and Synergistic Folding in Intrinsically Disordered Proteins with Amide H/D Exchange Mass Spectrometry. *Biochemistry* **2011**, *50*, 8722−8732.

(21) Cui, W.; Rohrs, H. W.; Gross, M. L. Top-Down Mass Spectrometry: Recent Developments, Applications and Perspectives. *Analyst* **2011**, *136*, 3854−3864.

(22) Clemmer, D. E.; Hudgins, R. R.; Jarrold, M. F. Naked Protein Conformations: Cytochrome *c* in the Gas Phase. *J. Am. Chem. Soc.* **1995**, *117*, 10141−10142.

(23) Shelimov, K. B.; Clemmer, D. E.; Hudgins, R. R.; Jarrold, M. F. Protein Structure in Vacuo: Gas-Phase Conformations of BPTI and Cytochrome *c*. *J. Am. Chem. Soc.* **1997**, *119*, 2240−2248.

(24) Hudgins, R. R.; Woenckhaus, J.; Jarrold, M. F. High Resolution Ion Mobility Measurements for Gas Phase Proteins: Correlation between Solution Phase and Gas Phase Conformations. *Int. J. Mass Spectrom. Ion Process.* **1997**, *165*−*166*, 497−507.

(25) Zilch, L. W.; Kaleta, D. T.; Kohtani, M.; Krishnan, R.; Jarrold, M. F. Folding and Unfolding of Helix-Turn-Helix Motifs in the Gas Phase. *J. Am. Soc. Mass Spectrom.* **2007**, *18*, 1239−1248.

(26) Wyttenbach, T.; Bowers, M. T. Structural Stability from Solution to the Gas Phase: Native Solution Structure of Ubiquitin Survives Analysis in a Solvent-Free Ion Mobility-Mass Spectrometry Environment. *J. Phys. Chem. B* **2011**, *115*, 12266−12275.

(27) Shelimov, K. B.; Jarrold, M. F. Conformations, Unfolding, and Refolding of Apomyoglobin in Vacuum: An Activation Barrier for Gas-Phase Protein Folding. *J. Am. Chem. Soc.* **1997**, *119*, 2987−2994.

(28) Wu, C.; Klasmeier, J.; Hill, H. H. Atmospheric Pressure Ion Mobility Spectrometry of Protonated and Sodiated Peptides. *Rapid Commun. Mass Spectrom.* **1999**, *13*, 1138−1142.

(29) Wyttenbach, T.; Von Helden, G.; Bowers, M. T. Gas-Phase Conformation of Biological Molecules Bradykinin. *J. Am. Chem. Soc.* **1996**, *118*, 8355−8364.
(30) McCullough, B. J.; Eastwood, H.; Clark, D. J.; Polfer, N. C.; Campopiano, D. J.; Dorin, J. A.; Maxwell, A.; Langley, R. J.; Govan, J. R. W.; Bernstein, S. L. Characterisation of Defb107 by Mass Spectrometry: Lessons From an Anti-Antimicrobial Defensin. *Int. J. Mass Spectrom.* **2006**, *252*, 180−188.
(31) Jurneczko, E.; Barran, P. E. How Useful Is Ion Mobility Mass Spectrometry for Structural Biology? The Relationship between Protein Crystal Structures and Their Collision Cross Sections in the Gas Phase. *Analyst* **2011**, *136*, 20−28.
(32) Skinner, O.; McLafferty, F.; Breuker, K. How Ubiquitin Unfolds after Transfer into the Gas Phase. *J. Am. Soc. Mass Spectrom.* **2012**, *23*, 1011−1014.
(33) Kalapothakis, J. M. D.; Berezovskaya, Y.; Zampronio, C. G.; Faull, P. A.; Barran, P. E.; Cooper, H. J. Unusual ECD Fragmentation Attributed to Gas-Phase Helix Formation in a Conformationally Dynamic Peptide. *Chem. Commun.* **2014**, *50*, 198−200.
(34) Zubarev, R. A.; Kelleher, N. L.; McLafferty, F. W. Electron Capture Dissociation of Multiply Charged Protein Cations. A Nonergodic Process. *J. Am. Chem. Soc.* **1998**, *120*, 3265−3266.
(35) Breuker, K.; Oh, H. B.; Lin, C.; Carpenter, B. K.; McLafferty, F. W. Nonergodic and Conformational Control of the Electron Capture Dissociation of Protein Cations. *Proc. Natl. Acad. Sci. U.S.A.* **2004**, *101*, 14011−14016.
(36) Breuker, K.; Brüschweiler, S.; Tollinger, M. Electrostatic Stabilization of a Native Protein Structure in the Gas Phase. *Angew. Chem.* **2011**, *50*, 873−877.
(37) Horn, D. M.; Breuker, K.; Frank, A. J.; McLafferty, F. W. Kinetic Intermediates in the Folding of Gaseous Protein Ions Characterized by Electron Capture Dissociation Mass Spectrometry. *J. Am. Chem. Soc.* **2001**, *123*, 9792−9799.
(38) Breuker, K.; Oh, H. B.; Horn, D. M.; Cerda, B. A.; McLafferty, F. W. Detailed Unfolding and Folding of Gaseous Ubiquitin Ions Characterized by Electron Capture Dissociation. *J. Am. Chem. Soc.* **2002**, *124*, 6407−6420.
(39) Oh, H.; Breuker, K.; Sze, S. K.; Ge, Y.; Carpenter, B. K.; McLafferty, F. W. Secondary and Tertiary Structures of Gaseous Protein Ions Characterized by Electron Capture Dissociation Mass Spectrometry and Photofragment Spectroscopy. *Proc. Natl. Acad. Sci. U.S.A.* **2002**, *99*, 15863−15868.
(40) Cooper, H. J.; Håkansson, K.; Marshall, A. G. The Role of Electron Capture Dissociation in Biomolecular Analysis. *Mass Spectrom. Rev.* **2005**, *24*, 201−222.
(41) Tuinstra, R. L.; Peterson, F. C.; Elgin, E. S.; Pelzek, A. J.; Volkman, B. F. An Engineered Second Disulfide Bond Restricts Lymphotactin/XCL1 to a Chemokine-like Conformation with XCR1 Agonist Activity. *Biochemistry* **2007**, *46*, 2564−2573.
(42) Peterson, F. C.; Elgin, E. S.; Nelson, T. J.; Zhang, F.; Hoeger, T. J.; Linhardt, R. J.; Volkman, B. F. Identification and Characterization of a Glycosaminoglycan Recognition Element of the C Chemokine Lymphotactin. *J. Biol. Chem.* **2004**, *279*, 12598−12604.
(43) Kuloglu, E. S.; McCaslin, D. R.; Kitabwalla, M.; Pauza, C. D.; Markley, J. L.; Volkman, B. F. Monomeric Solution Structure of the Prototypical 'C' Chemokine Lymphotactin. *Biochemistry* **2001**, *40*, 12486−12496.
(44) McCullough, B. J.; Kalapothakis, J.; Eastwood, H.; Kemper, P.; MacMillan, D.; Taylor, K.; Dorin, J.; Barran, P. E. Development of an Ion Mobility Quadrupole Time of Flight Mass Spectrometer. *Anal. Chem.* **2008**, *80*, 6336−6344.
(45) Mesleh, M. F.; Hunter, J. M.; Shvartsburg, A. A.; Schatz, G. C.; Jarrold, M. F. Structural Information from Ion Mobility Measurements Effects of the Long-Range. *J. Phys. Chem. A* **1996**, *100*, 16082−16086.
(46) Case, D.; Darden, T.; Cheatham, T., III; Simmerling, C.; Wang, J.; Duke, R.; Luo, R.; Walker, R.; Zhang, W.; Merz, K. *Amber 12*; University of California: San Francisco, CA, 2012.
(47) Lindorff-Larsen, K.; Piana, S.; Palmo, K.; Maragakis, P.; Klepeis, J. L.; Dror, R. O.; Shaw, D. E. Improved Side-Chain Torsion Potentials for the Amber Ff99sb Protein Force Field. *Proteins: Struct., Funct., Bioinf.* **2010**, *78*, 1950−1958.
(48) Roe, D. R.; Cheatham, T. E. PTRAJ and CPPTRAJ: Software for Processing and Analysis of Molecular Dynamics Trajectory Data. *J. Chem. Theory Comput.* **2013**, *9*, 3084−3095.
(49) Kuloglu, E. S.; McCaslin, D. R.; Markley, J. L.; Volkman, B. F. Structural Rearrangement of Human Lymphotactin, a C Chemokine, under Physiological Solution Conditions. *J. Biol. Chem.* **2002**, *277*, 17863−17870.
(50) Crown, S. E.; Yu, Y.; Sweeney, M. D.; Leary, J. A.; Handel, T. M. Heterodimerization of CCR2 Chemokines and Regulation by Glycosaminoglycan Binding. *J. Biol. Chem.* **2006**, *281*, 25438−25446.
(51) Handel, T. M.; Domaille, P. Heteronuclear (^{1}H, ^{13}C, ^{15}N) NMR Assignments and Solution Structure of the Monocyte Chemoattractant Protein-1 (MCP-1) Dimer. *Biochemistry* **1996**, *35*, 6569−6584.
(52) Seo, Y.; Andaya, A.; Bleiholder, C.; Leary, J. A. Differentiation of CC vs CXC Chemokine Dimers with GAG Octasaccharide Binding Partners: An Ion Mobility Mass Spectrometry Approach. *J. Am. Chem. Soc.* **2013**, *135*, 4325−4332.
(53) Sun, Q. Y.; Tyler, R. C.; Volkman, B. F.; Julian, R. R. Dynamic Interchanging Native States of Lymphotactin Examined By SNAPP-MS. *J. Am. Soc. Mass Spectrom.* **2011**, *22*, 399−407.
(54) Barran, P. E.; Polfer, N. C.; Campopiano, D. J.; Clarke, D. J.; Langridge-Smith, P. R. R.; Langley, R. J.; Govan, J. R. W.; Maxwell, A.; Dorin, J. R.; Millar, R. P.; Bowers, M. T. Is It Biologically Relevant to Measure The Structures of Small Peptides in the Gas-Phase? *Int. J. Mass Spectrom.* **2005**, *240*, 273−284.
(55) Harvey, S. R.; Porrini, M.; Tyler, R. C.; MacPhee, C. E.; Volkman, B. F.; Barran, P. E. To be submitted for publication.
(56) Roepstorff, P.; Fohlman, J. Proposal for a Common Nomenclature for Sequence Ions in Mass Spectra of Peptides. *Biomed. Mass Spectrom.* **1984**, *11*, 601.
(57) Iavarone, A. T.; Paech, K.; Williams, E. R. Effects of Charge State and Cationizing Agent on the Electron Capture Dissociation of a Peptide. *Anal. Chem.* **2004**, *76*, 2231−2238.
(58) Li, X.; Lin, C.; Han, L.; Costello, C. E.; O'Connor, P. B. Charge Remote Fragmentation in Electron Capture and Electron Transfer Dissociation. *J. Am. Soc. Mass Spectrom.* **2010**, *21*, 646−656.
(59) Sun, J.; Kitova, E. N.; Sun, N.; Klassen, J. S. Method for Identifying Nonspecific Protein−Protein Interactions in Nanoelectrospray Ionization Mass Spectrometry. *Anal. Chem.* **2007**, *79*, 8301−8311.